Impact of PC 71 BM layer on the performance of perovskite solar cells prepared at high moisture conditions using a low temperature annealed ZnO thin film as the electron transport…

Article *in* Journal of Materials Science: Materials in Electronics · November 2020

Carlos A. Rodríguez Castañeda
National Autonomous University of Mexico

D. Mateus Torres-Herrera
Center for Research and Advanced Studies of the National Polytechnic Institute

Hugo J. Cortina-Marrero
Universidad del Istmo

J Mater Sci: Mater Electron

Impact of $PC_{71}BM$ layer on the performance of perovskite solar cells prepared at high moisture conditions using a low temperature annealed ZnO thin film as the electron transport layer

Carlos A. Rodríguez-Castañeda[1,*], Paola M. Moreno-Romero[1], D. Mateus Torres-Herrera[1], Candy A. Enríquez-Alamares[2], Hugo J. Cortina-Marrero[2], I. Montoya De Los Santos[2], Maykel Courel[3], F. J. Sánchez-Rodríguez[4], Hailin Hu[1], and L. Hechavarría-Difur[2,*]

[1] *Instituto de Energías Renovables, Universidad Nacional Autónoma de México, C.P. 62580 Temixco, Morelos, Mexico*
[2] *Instituto de Estudios de La Energía, Universidad del Istmo, Santo Domingo Tehuantepec, C.P. 70760 Oaxaca, Mexico*
[3] *Centro Universitario de Los Valles, Universidad de Guadalajara, C.P. 46600, Ameca, Jalisco, Mexico*
[4] *Facultad de Ciencias Físico-Matemáticas, Universidad Autónoma de Sinaloa, C.P. 80010 Culiacán, Sinaloa, Mexico*

Received: 12 March 2020
Accepted: 27 October 2020

ABSTRACT

ZnO is a promising electron transport material with high electron mobility compared to TiO_2 and SnO_2. However, its high basicity and the presence of hydroxyl groups at the ZnO surface induces thermochemical decomposition of hybrid perovskites though proton transfer reactions. In perovskite solar cells (PSCs), these deprotonation reactions produce chemical products at the interface between ZnO and perovskite, which obstacle charge carrier extraction process and lead to low efficiency of the solar cells. In this work, $PC_{71}BM$ thin films of three different thickness, 19, 11 and 6 nm, were deposited on top of ZnO layers, prepared by sol–gel spin coating and annealed at 150 °C. It is found that low temperature prepared ZnO films contain deep trap states, and the effective optical band gap of ZnO/$PC_{71}BM$ double layers is slightly reduced with the thickness of the fullerene derivative. The presence of an interfacial $PC_{71}BM$ layer on top of ZnO enhances the stability of the upcoming perovskite coatings and promotes the passivation of trap states at the ZnO surface. Interestingly, the best $PC_{71}BM$-passivated PSC, fabricated under relative humidity (RH) of 60–65%, achieves a maximum power conversion efficiency (*PCE*) of 13.3%, whereas those PSCs with only ZnO as the electron transport layer show an average *PCE* of 5.5%. However, the stability under continuous illumination of $PC_{71}BM$ based PSCs is significantly lower than expected, probably due to the $PC_{71}BM$ degradation under high RH conditions.

Address correspondence to E-mail: carc@ier.unam.mx; lihed@live.com

https://doi.org/10.1007/s10854-020-04766-w

1 Introduction

Planar heterojunction hybrid perovskite solar cells (PSCs) have attracted extensive attention due to their exceptional power conversion efficiency (*PCE*) higher than 20% [1]. Part of the current progress is owing to development in different metal oxide electron-transport layers (ETL) such as TiO_2, WO_3, SnO_2, ZnO, in addition to organic molecules like fullerenes and their derivatives [2]. Because of the variety of ETL and the diverse issues or constraints referred to the efficient electron extraction and long-term stability [3, 4], surface and interface engineering methodology is a critical procedure to defect passivation and band alignment in order to improve charge transport process between the ETL/perovskite interface and the electrodes [5–7]. The performance of planar PSCs is quite sensitive to the interface properties, in particular the ETL surface at the n-i-p structure, which can influence the perovskite film morphology and crystallinity [8]. During the PSCs operation, photogenerated charge carries must transfer across the interfaces in order to be collected. Thus, the interfacial defects and the charge distribution considerably impact on the stability and performance of the PSCs [9].

Until now, several surface or interface organic modifiers deposited on top of the ETL have been reported. Among them, phenyl-C_{61}-butyric acid methyl ester ($PC_{61}BM$) thin film and buckminsterfullerene (C_{60}) as well as their combination ($PC_{61}BM + C_{60}$) have been used to modify the TiO_2/perovskite interface, facilitating the electron extraction and inhibiting the formation of trap states [10]. In WO_3, the surface modification by cesium carbonate (Cs_2CO_3)/$PC_{61}BM$ bilayer is used to reduce the charge recombination, improving the open circuit voltage (V_{oc}) and fill factor (*FF*). Likewise, C_{60} is used to passivate the grain boundaries in the perovskite films, resulting in a reduction of the hysteresis phenomena [11, 12]. On the other hand, a fullerene derivative, 9-(1-(6-(3,5-bis (hydroxymethyl) phenoxy) -1-hexyl) -1*H*-1,2,3-triazol-4-yl) -1-nonyl[60]-fullerenoacetate (C_9), is employed to suppress charge recombination and passivate the oxygen-vacancy-related defects on the surface of the SnO_2. The PSCs based on C_9-modified SnO_2, enhances the photogenerated charge extraction and improves the perovskite optoelectronic properties [13]. Eventually, the introduction of $PC_{61}BM$ as interface modifier in ZnO based PSCs, has been a reliable way to reduce de presence of hydroxyl groups at the ZnO semiconductor surface, alleviating the thermochemical decomposition of $CH_3NH_3PbI_3$ films and therefore reduced the interface defect states [14, 15].

Nevertheless, the fact that the organic modifications via fullerenes and their derivatives deposited on TiO_2, WO_3, SnO_2 and ZnO have led to remarkable advances for interlayers and improvements in the photovoltaic parameters, most of organic molecule based research for planar PSCs even still report the fabrication of high performance devices carried out in a well-controlled environment (nitrogen or argon filled glove box), which today results in high cost for eventual long-scale manufacturing [16, 17]. Moreover, the state-of-the-art progress towards high-performance metal oxide semiconductors as the ETL for PSCs, still remain in discussion. It is a well-known fact that, the deposition of the ETL require high-temperature processing (temperature > 350 °C) for an optimum film formation [18, 19]. Low-temperature processing metal oxide semiconductors exhibit poor electrical properties due to the presence of diverse defects and impurities [20, 21]. However, compared with other metal oxides, ZnO based films fabricated even at low-temperature processing can crystallize at approximately 150 °C, which is of particular interest when using flexible substrates [22]. Likewise, ZnO offers advantages as exceptional optical transparency and higher electron mobility than TiO_2, SnO_2 and WO_3 under the aforementioned conditions [23–25].

In this work, we propose the use of a ZnO thin film, fabricated at low temperature with a slow cooling procedure, as an electron transport layer in perovskite solar cells. Furthermore, the modification of the ZnO/$CH_3NH_3PbI_{3-x}Cl_x$ (perovskite) interface is carried out by a middle layer of 6-Phenyl C_{71} butyric acid methyl ester ($PC_{71}BM$) to promote the perovskite growth and avoid the thermochemical decomposition of $CH_3NH_3PbI_{3-x}Cl_x$ coating. The $PC_{71}BM$ deposition process consist in coating $PC_{71}BM$ solutions, prepared with different conditions, on top of ZnO films. The resultant samples were annealed at 100 °C for 10 min in a conventional oven. The procedure is totally performed in air under high relative humidity (RH) of 60–65%. We demonstrate that the intermediate $PC_{71}BM$ layer enhances the photovoltaic parameters of perovskite solar cells (PSCs). The average efficiency of ZnO based planar PSCs is increased in average from 5.5% to 12.9% when a $PC_{71}BM$ layer is inserted between ZnO and perovskite. Finally, the best PSC achieves a 13.3% *PCE* and retain 68.2% of its original efficiency after 100 mW cm^{-2} continuous irradiation for approximately 30 min under ambient conditions.

2 Experimental section

2.1 ZnO/$PC_{71}BM$ thin film deposition and characterization

The ZnO precursor was prepared by dissolving 109.75 mg zinc acetate dihydrate ($Zn(CH_3COO)_2$-$2H_2O$, Fermont, 99.9% ACS) and ethanolamine (MEA, Fluka, 99.0%) in a mixture of 10 µL acetylacetone ($CH_3COCH_2COCH_3$, Sigma-Aldrich, Reagent Plus 99%) and 1 mL 2-methoxyethanol (Sigma-Aldrich, 99.9%). The molar ratio of MEA/Zn was maintained at 1 and the concentration of zinc acetate was 0.5 M. The solution was magnetic stirred for 1 h at 60 °C until yielding a clear and homogeneous appearance. Afterward, the solution was aged for 12 h at room temperature prior to deposition. Zinc precursor solution was spin-coated onto clean glass or fluorine-doped tin oxide (FTO) coated glass slides at 3000 rpm for 30 s. Then, the coated samples were thermally treated in a furnace (Lindberg, ISB) at 150 °C for 3 h. The heating rate was 10 °C/min. ZnO film samples were left cooled down gradually to room temperature (slow cooling).

$PC_{71}BM$ ([6-Phenyl C_{71} butyric acid methyl ester, Sigma-Aldrich 99%) solutions were prepared by dissolving 10, 6 and 2 mg separately in 1 mL chlorobenzene (C_6H_5Cl, Sigma-Aldrich, ACS reagent, 99.5%), sample A, B and C, respectively. Each of them was magnetically stirred at 700 rpm during 1 h at 70 °C. $PC_{71}BM$ precursor solutions were dynamically spin-coated at 6000 rpm for 30 s on top of ZnO films. Then, the ZnO/$PC_{71}BM$ based films were annealed at 100 °C for 10 min in a conventional oven under atmosphere condition.

Thickness of ZnO and ZnO/$PC_{71}BM$ based films was estimated by contact profilometry using an Ambios XP 200 system. The thicknesses of ZnO and ZnO/$PC_{71}BM$ A, B and C double layers were: 37 nm, 56 nm, 48 nm and 43 nm, respectively. It suggested that the thickness of $PC_{71}BM$ A layer was about 19 nm, that of $PC_{71}BM$, about 11 nm, and $PC_{71}MB$ C, about 6 nm. Transmittance and reflectance spectra of film samples were analyzed in a Shimadzu 1800 UV–VIS spectrophotometer. The sheet electrical photoresponse of ZnO and ZnO/$PC_{71}BM$ samples was estimated with a Keithley 619 electrometer-multimeter and a Keithley 230 programmable voltage source unit under adjusted dark/light conditions. The electrical current–voltage (*I-V*) curves in the dark conditions of ZnO and ZnO/$PC_{71}BM$ films were measured using a digital Keithley 2400 four-wire source unit.

The photoluminescence (PL) spectra of the aforementioned films were obtained in a PerkinElmer LS-55 fluorescence spectrometer. X-Ray Diffraction (XRD) patterns of film samples were obtained by a Rigaku DMax-2200 system (Cu-Kα radiation with $\lambda = 0.15406$ nm) at 2θ detection angle from 5° to 70°. The pH value of the ZnO precursor solution was obtained in an Orion A_{series} Thermo Fisher Benchtop meter.

2.2 Perovskite solar cell fabrication and characterization

FTO coated glass substrates with a sheet resistance of 15 Ω/sq (Greatcell Solar) were partially etched with 1 M hydrochloric acid (HCl) and zinc powder, (Fermont, 99.3%). The etched FTO substrates were cleaned using Extran® MA 02 detergent, deionized water, acetone, and isopropyl alcohol [$(CH_3)_2CHOH$, IPA] in stages of 10 min and then dried by air flow. Later, the substrates were treated with a UV/Ozone ProCleaner® system for 20 min. Three types of ZnO/$PC_{71}BM$ based films were deposited on top of etched and cleaned FTO substrates by using the previous described procedure: ZnO/$PC_{71}BM$ A ($PC_{71}BM$ 10 mg mL^{-1}), ZnO/$PC_{71}BM$ B ($PC_{71}BM$ 6 mg mL^{-1}), ZnO/$PC_{71}BM$ C ($PC_{71}BM$ 2 mg mL^{-1}) and ZnO as reference.

To prepare the perovskite precursor solutions, 0.2 M methylammonium iodide (CH_3NH_3I or MAI, Lumtec, 99.5%) and 0.02 M methylammonium chloride (CH_3NH_3Cl or MACl, Lumtec, 99.5%), were dissolved in a mixture of 1 mL anhydrous IPA (Sigma-Aldrich, 99.5%) and 1 µL anhydrous *N,N*-dimethylformamide ($HCON(CH_3)_2$, DMF, Sigma-Aldrich, 99.8%). Likewise, 0.95 M PbI_2 (Lumtec, 99.9%) was dissolved in 1 mL DMF. Perovskite films were deposited by the spin-coating technique under ambient conditions with RH of approximately 60–65%. To achieve ideal deposition of PbI_2 on

$PC_{71}BM$ film, PbI_2 solution was first spin-coated dynamically at 3700 rpm for 40 s on top of ZnO/$PC_{71}BM$ films (also in ZnO). Then MAI + MACl solution was added dropwise as the spinning speed increased from 3700 to 4500 rpm for 10 s. This sequential procedure was performed in order to reduce the $PC_{71}BM$ film dissolution or delamination due to DMF solubility properties [26]. ZnO and ZnO/$PC_{71}BM$ with perovskite precursor coatings were annealed at 100 °C for 10 min in a conventional oven under atmosphere conditions. Scheme 1 exhibits such preparation process that was carried on in ambient conditions.

The hole transport layer (HTL) precursor solution was prepared by dissolving 80 mg Spiro-OMeTAD (Lumtec, 97%) in 750 μL of chlorobenzene (Sigma Aldrich, 99.5%), 28.8 μL of 4-tert-butylpyridine (Sigma Aldrich, 96%) and 16 μL of Li-TFSI solution, which consisted of 260 mg of Li-TFSI (Sigma Aldrich, 99.95%) in 500 μL of acetonitrile (Sigma Aldrich, 99%). 80 μL of the HTL precursor solution was spin-coated on top of perovskite films at 5000 rpm for 30 s in a nitrogen gas filled glove chamber. Later, samples were left drying in air for 12 h. Finally, samples were transferred to the thermal evaporator system, and 80 nm thick gold (Au) film was deposited at a rate of $1\ \text{Å}\ s^{-1}$ on top of the HTL layer at pressures below to 1×10^{-5} Torr.

Photocurrent density–voltage (*J-V*) curves of the perovskite solar cells were tested under ambient conditions using simulated AM 1.5G irradiation (100 mW cm^{-2}) through an Oriel 81,174 Class-AAA solar simulator. The light intensity was calibrated with a National Renewable Energy Laboratory-certified monocrystalline Si photodiode. Furthermore, a mask of 0.105 cm^2 defined the active illumination area of the devices. The number of total sweep points was 241, with a reverse scan direction from 1.1 to − 0.1 V and a forward scan direction from − 0.1 to 1.1 V. The solar cells were not pre-illuminated before the voltage scanning process.

3 Results and discussion

ZnO thin films annealed at 150 °C and cooled down slowly to room temperature show crystalline structure with (100), (002), (101), (102), (110), (103), (112) and (201) planes of polycrystalline hexagonal wurtzite crystal structure with no preferred orientation (Fig. S1). No other peaks are observed, suggesting that only single-phase ZnO has formed in these films. The cooling rate is quite important for the crystallinity of ZnO films. If the ZnO samples are suddenly cooled down from 150 °C to room temperature, the crystallinity would be reduced (Fig. S1) and the deep defect density would be increased, reflected in their photoconductivity (Fig. S2) and PL spectra (Fig.S3).

Steady-state PL spectra of the ZnO layers, with and without the $PC_{71}BM$ film and excited at 325 nm wavelength, are exhibited in Fig. 1. Reports suggest that the PL emission spectrum of ZnO consists of two emission bands, the ultraviolet (UV) emission band (370 to 400 nm) and a broad band in the visible region of the spectrum (400 nm to 700 nm) [27]. UV emission occurs due to the recombination of free excitons, which correspond to the energy difference between the top of the valence band (V_B) and the bottom of the conduction band (C_B) [28], and it appears in all samples. Moreover, the intensity of the UV emission peak of the ZnO thin film decreases when the thickness of the $PC_{71}BM$ layer is larger, which can be attributed to a non-radiative recombination process [29, 30]. Emissions in regions at approximately

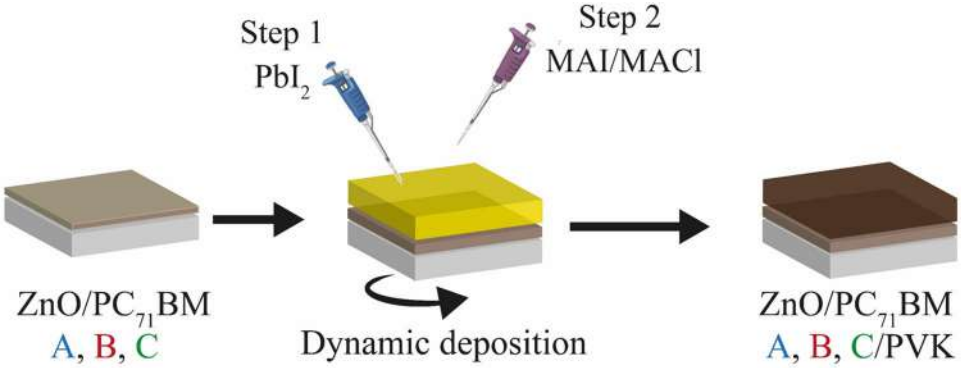

Scheme 1 Dynamic deposition process to prepare $PC_{71}BM$ layer on top of ZnO low-temperature films. Three types of $PC_{71}BM$ films are used: $PC_{71}BM$ A, $PC_{71}BM$ B, $PC_{71}BM$ C

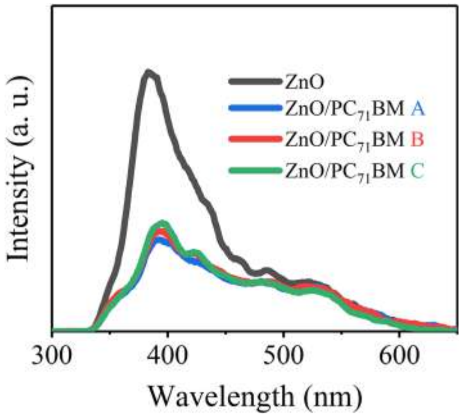

Fig. 1 Photoluminescence spectra of ZnO thin film and three types of ZnO/PC$_{71}$BM double layers

400 nm and 700 nm are known as deep-level emissions and denote the levels allowed within the forbidden band of the semiconductor. Likewise, the width of the band presumably comes from an overlap of several different deep-levels emitting at some quite close wavelengths [27, 31, 32].

The Gaussian fit of the steady-state PL spectra of the ZnO/PC$_{71}$BM based films which exhibit multiple peaks at the UV and visible regions are shown in Fig. 2. The deconvolution of these spectra gives a semi-quantitative description about the emission peaks at the UV region that appear at approximately 382 nm for ZnO and 395 nm for the ZnO/PC$_{71}$BM coated films. This emission is widely discussed in literature and it is commonly associated to different recombination mechanisms, such as, transitions related to structural defects or surface excitonic contribution [33, 34]. However, the emission bands at the visible range are not conclusive when using a PC$_{71}$BM interface modifier deposited on a low-temperature treated ZnO. We deduce that the blue-green luminescence region is associated with interstitial Zn (Zn$_i$) oxygen vacancies (V$_O$), oxygen interstitials (O$_i$), Zn vacancies (V$_{Zn}$) and antisite oxygen (O$_{Zn}$), as reported in literature [31, 35]. On the other hand, luminescence at the blue region is frequently associated to Zn$_i$ and V$_{Zn}$ defects in ZnO structures; the peak located at 419 nm is assigned to interstitial defects of Zn-to-Zn (Zn$_i$) [36]. The transition from the extended Zn$_i$ defects to the valence band causes the emission of peaks between 440 and 460 nm [30, 37]. The peak with the emission around 480 nm is associated with the transition between the Zn$_i$ level closest to the conduction band and the Zn vacancy levels formed near the valence band [29]. Furthermore, the emission peaks that appear between 480 and 508 nm are known as green emissions. Several reports propose that these emissions come from V$_O$ or V$_{Zn}$ [38–40]. As we shifted toward longer wavelengths in the spectrum, we observe yellow and orange emissions between 528 to 580 nm, which are probably transition induced at deep levels by neutral O$_{Zn}$/O$_i$ and ionized O$_i$, respectively [38]. Moreover, a new emission peak is observed in the PC$_{71}$BM coated films at approximately 565 nm, which can be attributed to interstitial oxygen (O$_i$).

The optical transmittance and reflectance spectra of ZnO, ZnO/PC$_{71}$BM and PC$_{71}$BM films, as well as the Tauc plots, were evaluated and presented in Fig. 3a and b, respectively. The absorption coefficient of the samples was calculated by the modified Lambert–Beer equation for transparent films. It is observed that a 3.02 eV of band gap (E_g) value is obtained for our ZnO layer. To prepare a low-temperature ZnO thin film, the pH value adjustment of the precursor solution with buffer solutions (pH 4–10) led to a remarkable reduction in the band gap value [41–43]. In our case the buffer solutions increased the pH value of the Zn precursor solutions from 7 to 8.7, which is the reason for a relatively low E_g value. On the other hand, the presence of PC$_{71}$BM reduces the transmittance spectra of ZnO/PC$_{71}$BM double layers between 390 and 600 nm, consequence of the optical absorption of PC$_{71}$BM. As a result, the effective E_g value of the double layers are 2.60, 2.65 and 2.68 eV for PC$_{71}$BM A, B and C based samples in that order. The increase of the effective E_g value is consistent with the decrease of the PC$_{71}$BM film thickness, 19, 11 and 6 nm, respectively.

The electrical properties of ZnO and ZnO/PC$_{71}$BM double films under direct bias voltage are measured at transversal and horizontal directions, as shown in Fig. 4a and b, respectively. The transversal configuration (inset of Fig. 4a), exhibit the measurement of differential electrical resistance (R_D) along the ZnO and ZnO/PC$_{71}$BM A, B, C thickness direction. In this case, the electrons move from one electrode to another through the entire thickness of the layers, which consist of 37 nm for ZnO, 56, 48 and 43 nm for ZnO/PC$_{71}$BM A, B, C double layer samples. Additionally, the *I-V* curve of a FTO substrate is included as reference. The values of R_D for each sample are obtained from the slope of the *I-V* curves at the lower voltage zone (< 0.3 V) and listed in Table 1. As

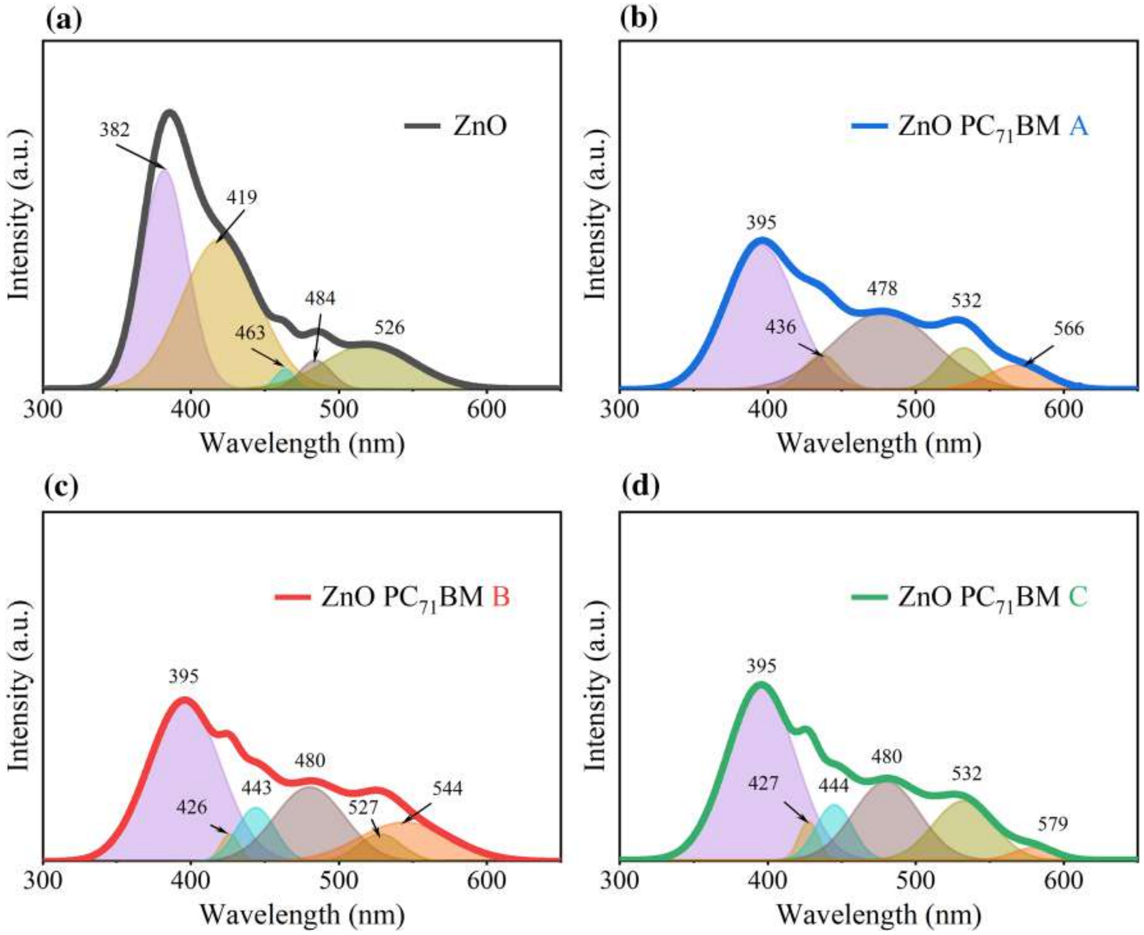

Fig. 2 Photoluminescence spectra with deconvolution of **a** ZnO **b** ZnO/PC$_{71}$BM A **c** ZnO/PC$_{71}$BM B **d** ZnO/PC$_{71}$BM C film samples

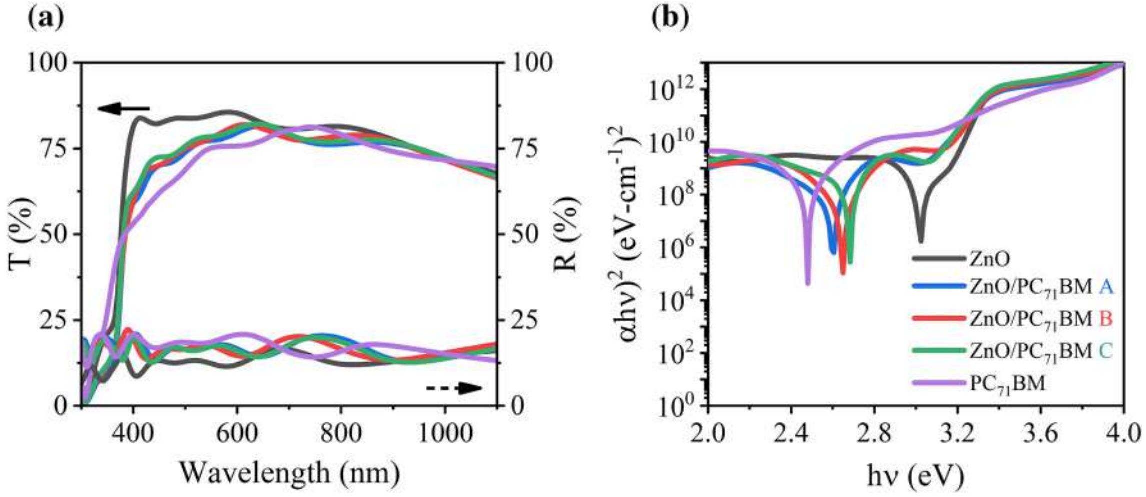

Fig. 3 **a** Transmittance (T) and reflectance (R) spectra of ZnO and ZnO/PC$_{71}$BM double layers **b** Tauc plots in logarithmic scale of ZnO and ZnO/PC$_{71}$BM double layers

expected, the R_D value of ZnO is lower than the ZnO/PC$_{71}$BM samples. The addition of the fullerene layer increases the ZnO resistance from 62.5 Ω to 309.6 Ω for 19 nm thick PC$_{71}$BM A, 127.6 Ω for 11 nm

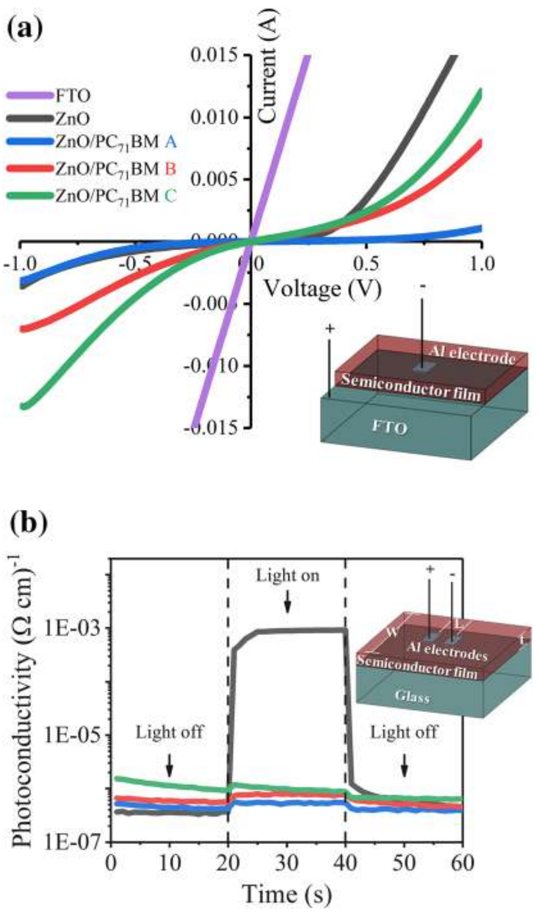

Fig. 4 **a** Transversal current–voltage (*I-V*, dark conditions) and **b** transient bulk or sheet electrical conductivity curves of ZnO and ZnO/PC$_{71}$BM based films. Insets: measurement schemes

thick PC$_{71}$BM B and 71.4 Ω for 6 nm thick PC$_{71}$BM C. We deduce that the interface resistance of ZnO/PC$_{71}$BM A (247.1 Ω) is larger than that of ZnO/PC$_{71}$BM C (8.9 Ω), which can increase the series resistance and affect the photovoltaic performance of the PSCs. Moreover, the *I-V* curves of the PC$_{71}$BM-modified ZnO films show a nonlinear rectification behavior at voltages out $-0.3 < V < 0.3$ range, similar to the non-ideal Schottky diodes. The *I-V* curves were fitted in the Schottky-diode current equation to obtain the ideality factor *n*. The ideality factor *n* values were greater than 10 for the entire ZnO and ZnO/PC$_{71}$BM based devices (16.6, 15.6, 14.3, 13.7 for ZnO and ZnO/PC$_{71}$BM A, B, C samples, respectively, see Supporting Information), which could be attributed to an accumulation of the electrical charge at the interface, as well as to the defects in the depletion region due to the polycrystalline structure of the ZnO films [43].

At horizontal configuration (inset of Fig. 4b), the current flows from one electrode to another through the surface of the film (single or bilayer). Figure 4b exhibits transient electrical photoconductivity of the ZnO and ZnO/PC$_{71}$BM based samples at 10 V bias voltage under non-illuminated conditions for the first 20 s, then under illumination for another 20 s, and under non-illumination once again for the last 20 s. It is observed that the photoconductivity of ZnO thin film is almost annihilated by non-photoconductive PC$_{71}$BM layers, as expected. The exposure to light under high moisture conditions could compromise the charge transport mechanisms in the ZnO/PC$_{71}$BM based samples by the formation of deep-level trap states [44]. We deduce that the electric characterization supports the presence of diverse defects discussed at the PL characterization. Furthermore, the slightly increased dark conductivity with the presence of PC$_{71}$BM suggest the possible surface passivation of low-temperature annealed ZnO films.

Steady-state PL spectra of the perovskite layers deposited on the ZnO substrates with and without PC$_{71}$BM are shown in Fig. 5. A perovskite film is included as reference. The perovskite emission peak (775 nm) is present in all ZnO/perovskite (PVK) samples and its intensity largely depends on the type of the underlayer. As discussed in the steady-state PL spectra characterization of the ZnO/PC$_{71}$BM based samples, a similar effect occurs attributed to non-

Table 1 Bulk or sheet conductivity and differential resistance of ZnO and ZnO/PC$_{71}$BM based films

Samples	Film thickness (nm)	Bulk conductivity, σ (Ω cm)$^{-1}$		Differential resistance, R_D (Ω)
		σ Dark	σ Light	
ZnO	37	3.66E-07	9.17E-04	62.5
ZnO/PC$_{71}$BM A	56	4.15E-07	5.50E-07	309.6
ZnO/PC$_{71}$BM B	48	5.61E-07	8.04E-07	127.6
ZnO/PC$_{71}$BM C	43	9.26E-07	1.17E-06	71.4

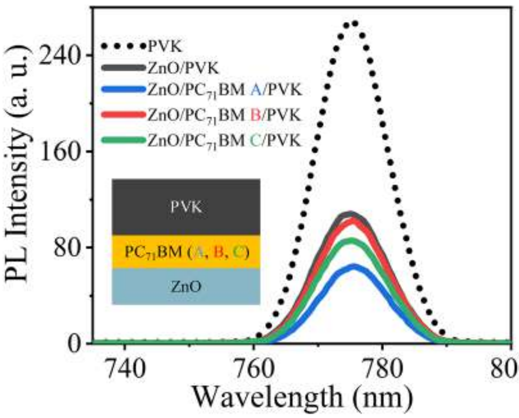

Fig. 5 Photoluminescence spectra of ZnO/PC$_{71}$BM/PVK multilayers annealed at 100 °C for 10 min, measured with the incident light on perovskite side. Substrates: FTO coated glass slide

radiative recombination of the system. It is observed that the intensity of the PL peak at 775 nm is significantly reduced when the perovskite is deposited on the ZnO and ZnO/PC$_{71}$BM A, B, C double layers. This reduction reflects the extraction of photogenerated charge carriers from the perovskite film to the ZnO layer. When inserting PC$_{71}$BM layers at the ZnO/PVK interface, the intensity of the PL peaks decreases even more, enhancing the charge transfer at the ZnO/PC$_{71}$BM interfaces and could promote an increment in the short-circuit current density in the PSCs, as will be seen later on.

The chemical stability of perovskite films deposited on the ZnO and ZnO/PC$_{71}$BM A, B, C double layers is evaluated by physical observation (photographs) and optical absorbance spectra, as showed in Fig. 6. The perovskite precursor films on top of ZnO and ZnO/PC$_{71}$BM based films were heated at 100 °C under ambient conditions (25 °C and RH of 70–80%) for 0, 5 and 15 min, to observe evidence of the degradation process at different annealing time. All samples exhibit a similar behavior and appearance in the optical absorption spectrum and photographs at the time 0. Figure 6a. Right after 5 min thermal treatment, a slight orange color is observed in all samples. These changes in the film samples exhibit the beginning of the PVK degradation process to a PbI_2 compounds. Likewise, the absorbance spectra show a slight decrease below 500 nm. Finally, after 15 min thermal treatment, further degradation is confirmed in the ZnO/PVK sample (Fig. 6b). It is noted that the samples with the fullerene coating exhibit lower degradation. However, an interesting effect to consider is the probability that the PC$_{71}$BM layers can agglomerate more by humidity when they are thicker (19 nm or 11 nm) than when they are thinner (6 nm), as observed in the photographs and the absorbance spectrum. The fact is that a thin PC$_{71}$BM layer could absorb less water, thus, reducing the PVK film degradation. Despite the protective effect provided by PC$_{71}$BM against the acid–base chemistry reaction at the interface of ZnO and perovskite, we conclude that the protection effect is lower than expected when the samples are exposed to high moisture conditions, as reported in literature [45].

Photovoltaic performance of ZnO and ZnO/PC$_{71}$BM A, B and C based PSCs is analyzed. The cell configuration is: FTO/ETL/PVK/Spiro OMeTAD/Au, where PVK means perovskite, and exhibited on the upper right of inset of Fig. 7a. Likewise, the energetic levels of the ZnO based planar PSCs is included in the same figure. Figure 7b shows the *J-V* curves of freshly prepared PSCs with ZnO, ZnO/PC$_{71}$BM A, ZnO/PC$_{71}$BM B, ZnO/PC$_{71}$BM C. Table 2 lists the average over 5 cell samples (Fig. S4) and maximum values of photocurrent density at short-circuit (J_{sc}), voltage at open-circuit (V_{oc}), fill factor (*FF*), and power conversion efficiency (*PCE*) in each type of PSCs. It is observed that ZnO-based PSCs exhibit an average efficiency 5.5%. However, the insertion of the PC$_{71}$BM interface modifier in the ZnO based PSCs results in an increment of the average efficiency. The best photovoltaic performance between the four types of the developed PSCs is found with ZnO/PC$_{71}$BM C, giving the highest *PCE* of 13.3%. These devices show an average J_{sc} of 21.61 mA cm^{-1}, V_{oc} of 0.92 V, *FF* of 0.65 and *PCE* of 12.9%, and have the smallest standard deviations of all the photovoltaic parameters.

Table 2 indicates that the average values of J_{sc}, V_{oc}, *FF* and *PCE* of the PSCs with ZnO/PC$_{71}$BM double layers depends significantly on the thickness of PC$_{71}$BM layer. The thicker the PC$_{71}$BM layer, the lower the photovoltaic parameters. The thickness of the PC$_{71}$BM layer influences on the series (R_s) and shunt resistance (R_{sh}) of the cells, exhibited in Table 2. It is observed that R_s value increases with the PC$_{71}$BM layer thickness, from 73 Ω of 6 nm thick PC$_{71}$BM C based PSCs, to 118 Ω of PC$_{71}$BM B based PSCs and 312 Ω of PC$_{71}$BM A based PSCs, which is consistent with the electrical resistance of the PC$_{71}$BM layer. On

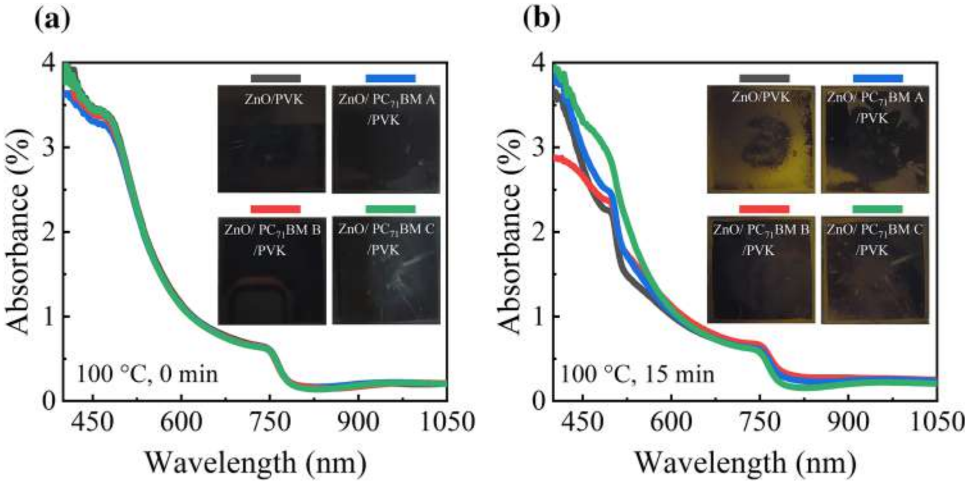

Fig. 6 Optical absorbance spectra and photographs of perovskite on top of ZnO/PVK, ZnO/PC$_{71}$BM A/PVK, ZnO/PC$_{71}$BM B/PVK and ZnO/PC$_{71}$BM C/PVK after thermal annealing at 100 °C for **a** 0 min, **b** 15 min. Substrates: Glass

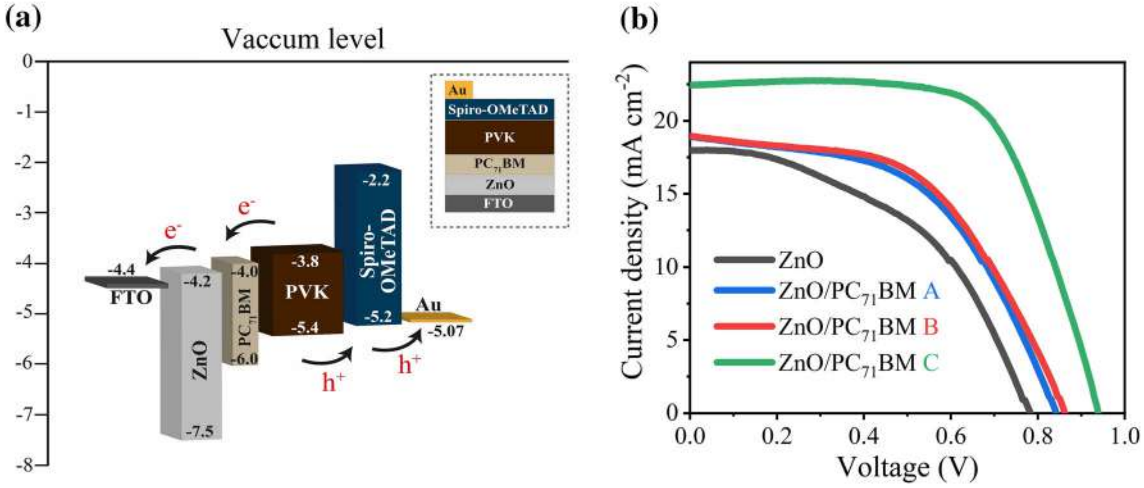

Fig. 7 **a** Energetic levels and schematic transversal section (inset) and **b** *J-V* curves of ZnO based planar perovskite solar cells: FTO/ETL/perovskite/Spiro-OMeTAD/Au solar cells, with four different ETL: ZnO, ZnO/PC$_{71}$BM A, ZnO/PC$_{71}$BM B, ZnO/PC$_{71}$BM C. PVK: perovskite

the contrary, R_{sh} reduces with the thickness of the PC$_{71}$BM films, from 11,130 to 2806 Ω, and its reduction should be related to the increase of the leak current or to the bimolecular recombination [46]. We believe that as the thickness of the PC$_{71}$BM layer increases, the probability of charge carrier recombination at that layer increment, leading to the reduction of R_{sh} values. It is well known that the increase of R_s values leads to the diminution of J_{sc} and *FF*, whereas the reduction of R_{sh} affects mainly on V_{oc} and *FF*. The tendencies of the two resistances are consistent with the photovoltaic parameters of the tested solar cells.

The reverse-forward scanned *J-V* curves of the PSCs are showed in Fig. S5, indicating relatively high hysteresis indices (HIs). The solar cells without PC$_{71}$BM exhibit the highest HI (61%), and the introduction of PC$_{71}$BM reduces such value down to 20%. The hysteresis in perovskite solar cells could be originated from different origins: ionic migration, capture and liberation of charge carriers in trap states, capacitive current and ferroelectric properties of perovskite [47]. It is reported that fullerene thin films could reduce (or eliminate) the hysteresis through passivation of trap states in inorganic semiconductors such as TiO$_2$ [48] and SnO$_2$ [49]. The reduction of hysteresis in this case suggests that PC$_{71}$BM makes contribution in the surface passivation of the low temperature annealed ZnO.

Even though the defects of ZnO are reduced by the incorporation of the PC$_{71}$BM modifier, the fullerene deterioration is inherent when oxygen and high

Table 2 Photovoltaic parameters and electrical resistances of the PSCs based on four different ZnO films; statistics of 5 cell samples: Average ± standard deviation (maximum)

Sample	J_{sc} (mA/cm^2)	V_{oc} (V)	*FF*	*PCE* (%)	R_s (Ω)	R_{sh} (Ω)
ZnO	16.56 ± 1.17 (18.17)	0.78 ± 0.03 (0.82)	0.42 ± 0.04 (0.47)	5.5 ± 0.5 (6.3)	71.5 ± 135.5 (121.5)	1042 ± 241 (1420)
ZnO/PC$_{71}$BM A	18.44 ± 0.75 (19.59)	0.80 ± 0.02 (0.84)	0.51 ± 0.02 (0.53)	7.6 ± 0.3 (7.9)	312.7 ± 0.3 (439.9)	2806 ± 1004 (4207)
ZnO/PC$_{71}$BM B	19.90 ± 1.12 (21.78)	0.90 ± 0.02 (0.93)	0.52 ± 0.04 (0.56)	8.3 ± 0.2 (8.6)	118.5 ± 9.6 (129.7)	3188 ± 1293 (4437)
ZnO/PC$_{71}$BM C	21.61 ± 0.81 (22.46)	0.92 ± 0.01 (0.93)	0.65 ± 0.01 (0.66)	12.9 ± 0.5 (13.3)	73.8 ± 2.1 (77.1)	11,130 ± 3258 (16,066)

moisture conditions are present. The stability of the PSCs could be reduced when they are exposed to long-term operation. The stability test was carried out at continuous illumination during about 30 min using a xenon lamp of 100 mW cm^{-2} of intensity on the four different types of ZnO-based PSCs. From Fig. 8, we confirm a decrease in the normalized J_{sc} and *FF* in approximately 20% when the PC$_{71}$BM modifier is incorporated. The normalized V_{oc} is not affected by the use of PC$_{71}$BM; it retains about 90% of its original value after the stability test. The total loss in *PCE* is about 20% without PC$_{71}$BM, and between 30 and 40% with PC$_{71}$BM after the continuous illumination in ambient conditions. It is important to mention that in previous studies it has been observed a photo-dimerization process in small organic molecules such as fullerenes under continuous illumination. This causes a transformation from a Van der Waals solid to one in which fullerenes are linked by covalent bonds [50]. Such transformation allows to the fullerenes be more resistant to a different solvent attack, however, prolonged light exposure can produce a significant reduction in charge carrier mobility which impact on *FF* and J_{sc} of the solar cells [51].

4 Conclusions

In this work, PC$_{71}$BM interface modifier, with a thickness between 6 and 19 nm, has been deposited on top of a 150 °C annealed ZnO thin film. According to photoluminescence analysis, the introduction of the PC$_{71}$BM interlayer promote changes on the defects of the ZnO surface. At a 380 nm wavelength, a reduction in the emission peak intensity is observed and attributed to passivation of trap states. The slow cooling rate is a quite important procedure to ensure the crystallinity and photoconductivity of the ZnO samples. The double ZnO/PC$_{71}$BM films exhibit optical transmittance of about 70–80% and the electrical conductivity ranges from 5.50×10^{-7} to 1.17×10^{-6} Ω cm^{-1}. The use of the 6 nm thick PC$_{71}$BM layer ensures an adequate separation within ZnO and perovskite and, at the same time, induces a minimum series resistance in order to achieve the best photovoltaic performance of 13.3% in the ZnO/PC$_{71}$BM based planar PSCs. Experimental results demonstrate that the PC$_{71}$BM layers suppress to a certain degree the thermal decomposition of perovskite at the proximity of ZnO. However, we

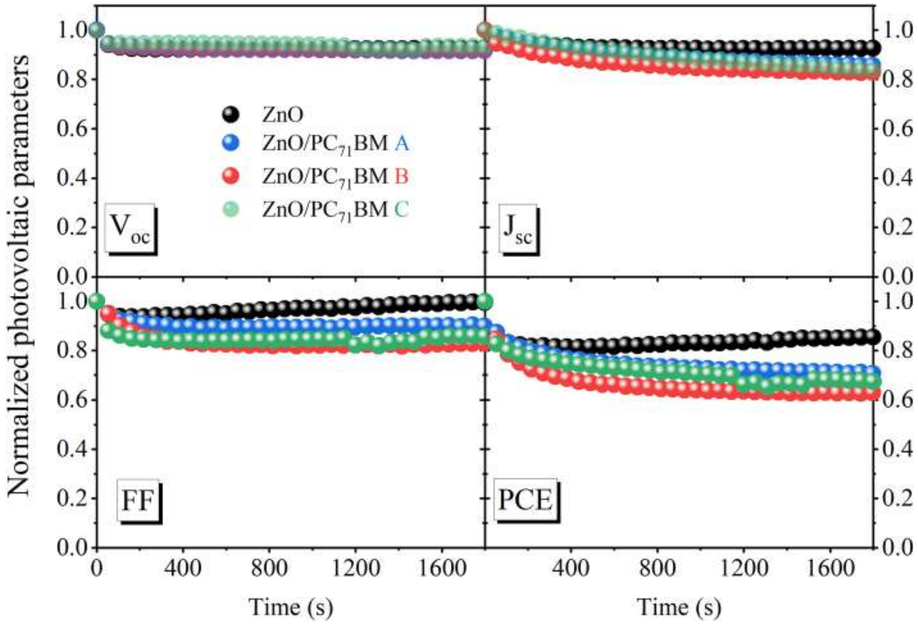

Fig. 8 Normalized photovoltaic parameters V_{oc}, J_{sc}, *FF* and *PCE*, of PSCs with 4 different types of ZnO under continuous illumination of about 30 min with a Xenon lamp of 100 mW cm^{-2}

observe that the protection effect of the PC$_{71}$BM interlayer under continuous illumination in a high RH ambient (60–65%) is lower than expected. ZnO based PSCs lose about 20% of its original efficiency after 30 min of continuous illumination, whereas such loss in ZnO/PC71BM based devices is about 30–40%. High humidity should play an important role in PC$_{71}$BM degradation.

Acknowledgements

The authors thank María Luisa Ramón-García for XRD measurements. CARC, DMTH and PMMR thank CONACyT-Mexico for graduate student scholarship. Financial supports from PRODEP project (DSA/103.5/16/10252) and UNAM PAPIIT (IN102619) are acknowledged.

Electronic supplementary material: The online version of this article (https://doi.org/10.1007/s10854-020-04766-w) contains supplementary material, which is available to authorized users.

References

1. M. Saliba, J.P. Correa-Baena, C.M. Wolff, M. Stolterfoht, N. Phung, S. Albrecht, D. Neher, A. Abate, Chem. Mater. **30**, 4193 (2018)
2. S. Zheng, G. Wang, T. Liu, L. Lou, S. Xiao, S. Yang, Sci. China Chem. **62**, 800 (2019)
3. G. Lu, X. Wang, J. Du, M. Zhang, Y. Gao, Y. Liu, J. Ma, Z. Lin, Coatings **10**, 46 (2020)
4. S.S. Shin, S.J. Lee, S.I. Seok, Adv. Funct. Mater. **29**, 1900455 (2019)
5. J. Ali, Y. Li, P. Gao, T. Hao, J. Song, Q. Zhang, L. Zhu, J. Wang, W. Feng, H. Hu, F. Liu, Nanoscale **12**, 5719 (2020)
6. J. Chen, N.-G. Park, ACS Energy Lett. **5**, 2742 (2020)
7. G. Yang, C. Wang, H. Lei, X. Zheng, P. Qin, L. Xiong, X. Zhao, Y. Yan, G. Fang, J. Mater. Chem. A **5**, 1658 (2017)
8. X. Guo, B. Zhang, Z. Lin, J. Ma, J. Su, W. Zhu, C. Zhang, J. Zhang, J. Chang, Y. Hao, Org. Electron. **62**, 459 (2018)
9. K. Choi, H. Choi, J. Min, T. Kim, D. Kim, S.Y. Son, G.-W. Kim, J. Choi, T. Park, Sol. RRL **4**, 1900251 (2020)
10. H. Pan, X. Zhao, X. Gong, H. Li, N.H. Ladi, X.L. Zhang, W. Huang, S. Ahmad, L. Ding, Y. Shen, M. Wang, Y. Fu, Mater. Horizons **7**, 2276 (2020)
11. V.O. Eze, Y. Seike, T. Mori, Org. Electron. **46**, 253 (2017)
12. C.-M. Chen, Z.-K. Lin, W.-J. Huang, S.-H. Yang, Nanoscale Res. Lett. **11**, 464 (2016)
13. K. Liu, S. Chen, J. Wu, H. Zhang, M. Qin, X. Lu, Y. Tu, Q. Meng, X. Zhan, Energy Environ. Sci. **11**, 3463 (2018)
14. F. Qin, W. Meng, J. Fan, C. Ge, B. Luo, R. Ge, L. Hu, F. Jiang, T. Liu, Y. Jiang, Y. Zhou, A.C.S. Appl, Mater. Interfaces **9**, 26045 (2017)
15. Q. Dong, C.H.Y. Ho, H. Yu, A. Salehi, F. So, Chem. Mater. **31**, 6833 (2019)

16. F. Wang, Y. Zhongbiao, H. Sarvari, S. Park, K. Graham, Y. Zhao, and Z. David Chen, in *2017 IEEE 44th Photovolt. Spec. Conf.* (IEEE, 2017), pp. 1044–1047.
17. M. F. Mohamad Noh, N. A. Arzaee, I. N. Nawas Mumthas, N. A. Mohamed, S. N. F. Mohd Nasir, J. Safaei, A. R. bin M. Yusoff, M. K. Nazeeruddin, and M. A. Mat Teridi, (2020) J. Mater. Chem. A **8**: 10481
18. N. Tiwari, A. Nirmal, M.R. Kulkarni, R.A. John, N. Mathews, Inorg. Chem. Front. **7**, 1822 (2020)
19. Z. Cao, C. Li, X. Deng, S. Wang, Y. Yuan, Y. Chen, Z. Wang, Y. Liu, L. Ding, and F. Hao, J. Mater. Chem. A (2020).
20. M.A. Haque, A.D. Sheikh, X. Guan, T. Wu, Adv. Energy Mater. **7**, 1602803 (2017)
21. S.-H. Chan, Y.-H. Chang, M.-C. Wu, Front. Mater. **6**, 1 (2019)
22. H. Chen, H. Wang, J. Wu, F. Wang, T. Zhang, Y. Wang, D. Liu, S. Li, R.V. Penty, I.H. White, Nano Res. **13**, 1997 (2020)
23. P. Zhang, J. Wu, Y. Wang, H. Sarvari, D. Liu, Z.D. Chen, S. Li, J. Mater. Chem. A **5**, 17368 (2017)
24. H. Mun, H. Yang, J. Park, C. Ju, K. Char, APL Mater. **3**, 076107 (2015)
25. G. Zheng, J. Wang, H. Liu, V. Murugadoss, G. Zu, H. Che, C. Lai, H. Li, T. Ding, Q. Gao, Z. Guo, Nanoscale **11**, 18968 (2019)
26. P. Cheng, Y. Li, X. Zhan, Nanotechnology **24**, 484008 (2013)
27. A. Galdámez-Martinez, G. Santana, F. Güell, P.R. Martínez-Alanis, A. Dutt, Nanomaterials **10**, 857 (2020)
28. K. Kodama, T. Uchino, J. Appl. Phys. **111**, 093525 (2012)
29. A. Ali, G. Rahman, T. Ali, M. Nadeem, S.K. Hasanain, M. Sultan, Phys. E Low-Dimensional Syst. Nanostructures **103**, 329 (2018)
30. K. Yuan, L. Chen, F. Li, Y. Chen, J. Mater. Chem. C **2**, 1018 (2014)
31. S.A. Studenikin, N. Golego, M. Cocivera, J. Appl. Phys. **84**, 2287 (1998)
32. A. Mahroug, S. Boudjadar, S. Hamrit, L. Guerbous, J. Mater. Sci. Mater. Electron. **25**, 4967 (2014)
33. O. Marin, M. Tirado, N. Budini, E. Mosquera, C. Figueroa, D. Comedi, Mater. Sci. Semicond. Process. **56**, 59 (2016)
34. J. Rodrigues, D. Smazna, N. Ben Sedrine, E. Nogales, R. Adelung, Y. K. Mishra, B. Mendez, M. R. Correia, T. Monteiro (2019) Nanoscale Adv. **1**: 1516
35. N.E. Hsu, W.K. Hung, Y.F. Chen, J. Appl. Phys. **96**, 4671 (2004)
36. Z.W. Ai, Y. Wu, H. Wu, T. Wang, C. Chen, Y. Xu, C. Liu, Nanoscale Res. Lett. **8**, 105 (2013)
37. H. Zeng, G. Duan, Y. Li, S. Yang, X. Xu, W. Cai, Adv. Funct. Mater. **20**, 561 (2010)
38. R.K. Biroju, P.K. Giri, J. Appl. Phys. **122**, 044302 (2017)
39. B. Lin, Z. Fu, Y. Jia, Appl. Phys. Lett. **79**, 943 (2001)
40. M. Wang, Y. Zhou, Y. Zhang, E. Jung Kim, S. Hong Hahn, S. Gie Seong, Appl. Phys. Lett. **100**, 101906 (2012)
41. R. Haarindraprasad, U. Hashim, S.C.B. Gopinath, M. Kashif, P. Veeradasan, S.R. Balakrishnan, K.L. Foo, P. Poopalan, PLoS ONE **10**, e0132755 (2015)
42. K. Sivakumar, V. Senthil kumar, N. Muthukumarasamy, M. Thambidurai, T.S. Senthil, Bull. Mater. Sci. **35**, 327 (2012)
43. C. Zhou, A. Ghods, K. L. Yunghans, V. G. Saravade, P. V. Patel, X. Jiang, B. Kucukgok, N. Lu, and I. Ferguson, in edited by F. H. Teherani, D. C. Look, and D. J. Rogers (2017), p. 101051K.
44. S. Wilken, J. Parisi, H. Borchert, J. Phys. Chem. C **118**, 19672 (2014)
45. J. Yang, B.D. Siempelkamp, E. Mosconi, F. De Angelis, T.L. Kelly, Chem. Mater. **27**, 4229 (2015)
46. R. Singh, S. Sandhu, J.-J. Lee, Sol. Energy **193**, 956 (2019)
47. B. Chen, M. Yang, S. Priya, K. Zhu, J. Phys. Chem. Lett. **7**, 905 (2016)
48. K. Wojciechowski, S.D. Stranks, A. Abate, G. Sadoughi, A. Sadhanala, N. Kopidakis, G. Rumbles, C.-Z. Li, R.H. Friend, A.K.-Y. Jen, H.J. Snaith, ACS Nano **8**, 12701 (2014)
49. W. Ke, D. Zhao, C. Xiao, C. Wang, A.J. Cimaroli, C.R. Grice, M. Yang, Z. Li, C.-S. Jiang, M. Al-Jassim, K. Zhu, M.G. Kanatzidis, G. Fang, Y. Yan, J. Mater. Chem. A **4**, 14276 (2016)
50. P.C. Eklund, A.M. Rao, P. Zhou, Y. Wang, J.M. Holden, Thin Solid Films **257**, 185 (1995)
51. A. Distler, T. Sauermann, H.-J. Egelhaaf, S. Rodman, D. Waller, K.-S. Cheon, M. Lee, and D. M. Guldi, Adv. Energy Mater. **4**, n/a (2014).